The Age and Metallicity of the Boötes I System

Joanne Hughes

Physics Department, Seattle University, Seattle, WA 98122

jhughes@seattleu.edu

George Wallerstein

Astronomy Department, University of Washington, Box 351580, Seattle, WA 98195-1580

and

Anne Bossi

Physics Department, Seattle University, Seattle, WA 98122

ABSTRACT

We present Washington CT_1T_2 photometry of a field central to the Boötes I dwarf spheroidal galaxy, which was discovered as a stellar overdensity in the Sloan Digital Sky Survey (DR5). We show that the Washington filters are much more effective than the Sloan filters in separating the metal-poor turn-off stars in the dwarf galaxy from the foreground stars. We detect 165 objects in the field, and statistically determine that just over 40% of the objects are non-members. Our statistical analysis mostly agrees with radial velocity measurements of the brighter stars. We find that that there is a distinct main-sequence turn-off and subgiant branch, where there is some evidence of a spread in chemical abundance. Any evidence of an age spread is limited to a few billion years. The brightest 7 Boötes I members give a (photometric-color derived) weighted mean iron-abundance of $[Fe/H] = -2.1^{+0.3}_{-0.5}$, and the best-fit isochrone is the 14.1 Gyr, Z=0.0002 model, with $(m-M)_V = 19.11$ and $E(B-V) = 0.02$.

Subject headings: galaxies: dwarf; galaxies: individual – (Boötes I) – Local Group

1. Introduction

Over the last few years, the Sloan Digital Sky Survey (SDSS, York et al. 2000) has been mined for stellar overdensities, leading to the discovery of many new systems which have the broad characteristics of dwarf galaxy-satellites of the Milky Way. In addition to Boötes I (Belokurov et al. 2006a), we also include Boötes II (Walsh et al. 2007), Canes Venatici (Zucker et al. 2006a), Willman 1 (Willman et al. 2005a), Ursa Major (Willman et al. 2005b), Ursa Major II (Zucker

et al. 2006b), Hercules, Coma Berenices, SEGUE 1, Canes Venatici II, Leo IV (Belokurov et al. 2006b).

Belokurov et al. (2006a, hereafter B06) describe the method used to search the SDSS *ugriz* data for stellar overdensities. They also performed follow-up observations with the 4-m Blanco Telescope at the Cerro Tololo Inter-American Observatory in Chile of a $36' \times 36'$ field in the g and i bands. B06 compared the color-magnitude diagram (CMD) of Boötes I with that of the metal-poor galactic globular cluster, M92. Their deep (wide-field) Boötes I CMD is very crowded near the main sequence turn-off, but B06 use the fiducial ridgeline of M92 to state that Boötes I is younger and slightly more metal-poor than M92 (for which $[Fe/H] \sim -2.3$). The characteristic scale length of Boötes I was found to be about 220 pc at a distance of about 60 kpc. This distance is similar to that of the outermost halo globular clusters in our galaxy, closer than that of most of our accompanying dwarf galaxies which reside at distances of about 100 kpc (accompanied by a few globulars). This preliminary work shows that the dwarf galaxy is distorted (from the density contours), which suggests that it may be experiencing tidal disruption. At $M_V \ -5.8\, mag$, Boötes I is one of the faintest dSphs found to date, and one of the closest.

Muñoz et al. (2006) took spectra of red giant branch (RGB) and asymptotic giant branch (AGB) stars (selected from SDSS DR4, because of proprietary issues at the time) in the core of Boötes I and south of declination 14.8°. The radial velocity data on the stars did not clearly distinguish the Boötes I population from the Milky Way stars, so they used spectroscopic features to remove foreground stars. Their data (for only 7 stars) yielded a systematic velocity of $95.6 \pm 3.4\ km/s$, a central velocity dispersion of $6.6 \pm 2.3\ km/s$, and a mass of $1.1^{+1.3}_{-0.5} \times 10^7 M_\odot$. Muñoz et al. (2006) have found that Boötes I is not only one of the faintest known dSphs, but also one of the darkest (M/L ratio of between 130–680), and most metal poor, at $[Fe/H] \sim -2.5$. Martin et al. (2007) observed candidate Boötes I red giants from SDSS (DR4) with Keck/DEIMOS, converting measurements of the Ca II lines to $[Fe/H]$, finding $99.9 \pm 2.4\ km/s$, with central velocity dispersion $\sigma = 6.5^{+2.1}_{-1.3}\ km/s$ for their final sample of 24 stars with small velocity uncertainties. For the DEIMOS sample, $[Fe/H] \sim -2.1$, with one star at -2.7. Martin et al. (2007) discuss the systematic uncertainties involved, and part of the reason their data seems to skew more metal-rich than Muñoz et al. (2006) (and Siegel 2006) may be due to Martin et al. using the Caretta & Gratton (1997) metallicity scale rather than that of Zinn & West (1984). However, Martin et al. note that none of the groups doing spectroscopy were using techniques which had been calibrated below $[Fe/H] \sim -2.3$, so the discrepancies might stem from that factor.

Siegel (2006) and Dall'Ora et al. (2006) have studied variable stars in Boötes I. Using the McDonald Observatory 0.8-m telescope and B, Washington M, T_2 (I-band), and DDO51 filters, Siegel (2006) identified 15 RR Lyrae stars, and estimated the distance to Boötes I as $(m - M)_0 = 18.96 \pm 0.12$, using $E(B - V) = 0.056$, with $-2.5 < [Fe/H] < -2.0$. From 58 B-images, Siegel found the average *RRab* period to be 0.69 days (period shift -0.07, compared with M3 RR Lyraes), with 53% being type c pulsators, and classifying it as an Oosterhoof type II system (rather than *intermediate,* as for other dSphs, except Ursa Minor), which also implies it is very metal-poor.

Siegel's CMD was in (B-I), with the M-DDO51 colors used to remove field dwarfs. Dall'Ora et al. (2006) presented the V,I light curves of 12 variables, 11 of which were RR Lyraes. They find the distance modulus to be $19.11 \pm 0.08\ mag$ for the assumed metal abundance of $[Fe/H] \sim -2.5$ and $E(B-V) = 0.02$, which we use as our distance modulus and extinction values in this paper. Unfortunately, these variable stars fell outside our central field.

Recently, de Jong et al. (2008) performed a numerical analysis of the SDSS CMDs of several dSphs and globular clusters, using the new software package MATCH. They found that the Boötes I SDSS data was consistent with the population being old and metal-poor, with no evidence of more than one burst of star formation. The CMD-analysis only showed CVn I, UMa II, and Leo T having more than one epoch of star formation, but the conclusions were drawn from SDSS-data only,

We have obtained photometry in the Washington filters to investigate the main sequence turn-off (MSTO) and subgiant branch (SGB) of Boötes I. The CT_1T_2 photometry provides metallicity as well as temperature information for the cluster's giants and subgiants. The position of the RGB is metallicity-dependent, but we examine the MSTO/SGB region to search for evidence of age spreads.

2. Observations

We observed one field centered on ($RA = 14^h00^m06^s$, $Dec = 14.5°$; *J2000)* with the Apache Point Observatory 3.5-m telescope, using the direct imaging SPIcam system. The detector is a backside-illuminated SITe TK2048E 2048×2048 pixel CCD with 24 micron pixels, which we binned (2×2), giving a plate scale of 0.28 arcseconds per pixel, and a field of view of 4.78×4.78 square arcminutes. The data set for Boötes I was taken on 2007 March 19. We took 21 frames in Washington C, and Cousins R and I filters, with exposure time ranging from 1 seconds to 1000 seconds. The readout noise was 5.7e- with a gain of 3.4 e-/ADU. The images were flat-fielded using dome flats, along with a sequence of zeros. We then processed the images using the image-processing software in IRAF.

As we described in Hughes et al. (2007; studying the bulge globular cluster, NGC 6388), we substituted R- and I-filters for Washington T_1 and T_2, because $(R-I)$ can be converted to $(T_1 - T_2)$ linearly. R & I are broader than Washington T_1 and T_2, which reduces the observing time, and the Washington C-filter is much broader than the B-band of the UBV system as well as the Strömgren v-band. The C-band is also more sensitive to metallicity than the B-filter. Due to these factors, we prefer the Washington filters over the more commonly used BVRI-filters. Geisler & Sarajedini (1999) explained the advantages that the Washington system provides: they widen the separation of the giant branches of different metallicities (giving a resolution for RGB fiducials of $\sim 0.15\ dex$), while the reddening sensitivity of the Washington filters is half that of the (V-I) colors. In this paper, we use the "New Washington System CCD Standard Fields", SA 101 and SA

107 (Geisler 1996), the standard giant branches of Geisler & Sarajedini (1999; hereafter, GS99), and the theoretical models of Marigo et al. (2008). We note that Sneden et al. (2000) find that M15 and M92 have a similar abundances, $[Fe/H] \sim -2.3$, wheras the -2.15 of GS99 comes from Zinn (1985).

Our photometry on 2007 March 19 yielded matches to the GS99 standard system of $\sigma_{rms} = 0.011$ in T_1, $\sigma_{rms} = 0.023$ in C, and $\sigma_{rms} = 0.017$ in T_2. In T_1, the average uncertainties in the final CMD were $\sigma_{rms} \leq 0.03$ at the level of the horizontal branch, and $\sigma_{rms} = 0.05$ just above the MSTO. The transformation equations are as follows:

$$T_1 = R_i - 0.289 + 0.023(C_i - R_i) - 0.206X,\ \sigma_{rms} = 0.011 \quad (1)$$

$$C = C_i - 1.320 + 0.128(C_i - R_i) - 0.396X,\ \sigma_{rms} = 0.023 \quad (2)$$

$$T_2 = I_i - 0.768 + 0.006(R_i - I_i) - 0.087X,\ \sigma_{rms} = 0.017 \quad (3)$$

Here, X denotes the airmass and the subscript i indicates the instrumental magnitude.

Table 1 lists the data taken in spring, 2007 at APO. The images taken on 2007 March 19 had sub-arcsecond seeing. We did take data on an offset Boötes I field and an off-dSph region at the same galactic latitude on the night of UT 2008 January 14, but the seeing was 2-3″ and variable. We use the "foreground" field for non-member selection, but we do not include the extra Boötes I field because the data were of much poorer quality.

We used the DAOPHOT program in IRAF (Stetson et al. 1990) to perform crowded field photometry, although it was scarcely necessary for this sparsely populated field (compared to a globular cluster) of the Boötes I dwarf. Artificial-star experiments found that for the deepest C-frames, and the 300-s R and I exposures, nearly all the artificial objects placed in the field (except close to the bright foreground stars) were recovered (adding about 20% to the total number of detections, with a range of magnitudes from 16–22 in T_1).

We used two iterations of (DAOPHOT-PHOT-ALLSTAR), with the first iteration having a detection threshold of 4σ, and the second pass had a 5σ detection limit. We used 10-15 stars to construct the point spread functions (PSFs), and did not allow it to vary over the chip (there was clear evidence that the PSF was constant over the whole frame anyway). ALLSTAR was further constrained to only detect objects with a CHI-value (the DAOPHOT goodness-of-fit statistic) between 0.5 and 1.5 (to remove cosmic rays and non-stellar, extended objects). We found the aperture correction between the small (3 pixel) aperture used by ALLSTAR in the Boötes I field, and the larger (10 pixel) aperture used for the standards, by using the PSF stars in each image. We used the IMMATCH programs to match the source lists in each frame, which resulted in several data sets in C, T_1 & T_2. We then put together the final source list as follows: requiring that each star be detected in at least one image in each filter, and the final magnitude and colors were calculated as the weighted mean of each individual detection We calculated uncertainties for each individual object in each frame by taking the uncertainties from photon statistics, DAOPHOT's uncertainties,

the aperture corrections, and the standard photometric errors in quadrature. Figure 1 shows the total uncertainties in T_1, $(C - T_1)$ and $(T_1 - T_2)$ against the T_1-magnitude.

3. Boötes I Membership

Figure 2a shows Washington CMD of the 165 stars (listed in Table 2). In Figure 2b, we display the data set with the standard giant branches of GS99 (having marked values of [Fe/H]), where M15 (GS99) data (small circles) are shown for comparison. We use the distance modulus of 19.11 and $E(B-V) = 0.02$. To convert from $E(B-V)$ to the reddening in the Washington filters we used: $E(C-T_1) = 1.966E(B-V)$; $E(T_1-T_2) = 0.692E(B-V)$; $M_{T_1} = T_1 + 0.58E(B-V) - (m-M)_V$; from Geisler, Claria & Minniti (1991) and GS99. We note that care should be taken in areas of suspected variable extinction (see discussion in Hughes et al. 2007, for NGC 6388). Twarog et al. (2006) state that a small shift of only 0.05 in $E(B-V)$ increases the Washington-$[Fe/H]$ from -0.57 to -0.35 for Melotte 71. Fortunately, the small extinction value of $E(B-V) \sim 0.02$, (Dall'Ora et al. 2006) and high galactic latitude, reduces this possibility for Boötes I. We plot the Boötes I stars (open squares) with their error bars, and note that there are at least 4-6 stars in the blue straggler region, brighter and bluer than the main-sequence turn-off. Our photometry does not appear to have any color-shifts with respect to the M15 data from GS99, which has $(m-M)_V = 15.41$ and $E(B-V) = 0.10$.

Our method of using three Washington filters, CT_1T_2, is meant to provide more than one color to determine Boötes I membership. As demonstrated by Siegel, Shetrone & Irwin (2008) for Willman 1, follow-up studies showed that many of the brightest stars thought to be part of that system's RGB, were dwarf stars and halo objects. For future follow-up spectroscopy, we want to know whether the Boötes I RGB stars really belong to the dSph.

In an ideal situation, we would have obtained exactly the same number of frames in each filter on the off-galaxy field (at the same galactic latitude), on the same night, under the same seeing conditions. However, we obtained frames of an offset Boötes I field and an off-galaxy field on 2008 January 14, with integration times of 180s at I, 240s at R and 360s at C. These data only reached the base of the RGB, with seeing of 2–3 arcseconds, compared to sub-arcsecond seeing on 2007 March 19. We did detect 14 objects in the off-galaxy field compared with 34 in the offset Boötes I field. We show these objects as open stars in Figure 3. This CMD also shows the M15 objects (GS99, small circles) and the proposed Boötes I stars (filled squares). Since the off-galaxy field could not go deep enough to reach the Boötes I MSTO, we used the TRILEGAL 1.1 code (see Girardi et al. 2005), which simulates photometry (in many filter combinations) for any galactic field. We ran the code, using the web interface,[1] for the same area as our Boötes I field, with the same limiting magnitude in T_1. The run with the standard galactic parameters (A_V, IMF, e.t.c.,

[1] http://stev.oapd.inaf.it/cgi-bin/trilegal

see Girardi et al. 2005) yielded 76 simulated objects (shown as crosses in Figure 3), which can now be treated as foreground contaminating stars. From the initial numbers in the real and simulated fields, we expect at least 40% of the on-Boötes I source list to be foreground objects, mostly in the giant branches, not the MSTO region. As a first cut in the *cleaning* process, Figure 3 shows that the M15 data and the Boötes I MSTO are best fit by the Z=0.0002, 14.1 Gyr isochrone of Marigo et al. (2008).[2] It is likely that none of the Boötes I members fall beyond the Z=0.0006, 12.7 Gyr isochrone.

Figure 4 is the $(T_1 - T_2)$ vs. $(C - T_1)$ color-color plot of the Boötes I stars with uncertainties better than 0.05, shown as filled squares, the off-galaxy field objects are open stars, and the simulated foreground objects are crosses. The constant-$[Fe/H]$ lines from Geisler, Claria & Minniti (1991) are marked. The Z=0.0006, 12.7 Gyr, isochrone of Marigo et al. (2008) is also drawn, showing that the sub-giant and MSTO stars that do not share the colors of the foreground objects, stay to the metal-poor side of this line. This color-color plot is only sensitive to metallicity, as all the isochrones at the same Z fall in the same locus. Foreground dwarfs with red $(T_1 - T_2)$ vs. $(C - T_1)$ colors do occupy the locus of the metal-poor RGB-tip stars, which was the case with Willman 1 (Siegel, Shetrone & Irwin 2008). Thus, Figure 4 shows that resorting to cuts in color would only be successful at the MSTO to the base of the RGB. As we have done with NGC 6388 & ω Cen (Hughes et al. 2007; Hughes & Wallerstein 2000), we can statistically compare the off-galaxy region (and the simulated field) to the Boötes I field. We subtract the foreground stars statistically by the following method, used by Hughes & Wallerstein (2000), which was adapted from Mighell, Sarajedini, & French (1998).

We calculate the probability that the star in the Boötes I field CMD is a member of the dSph population as:

$$p \approx 1 - min\left(\frac{\alpha N_{off}^{UL\,84}}{N_{on}^{LL\,95}},\ 1.0\right) \tag{4}$$

Where α is the ratio of the area of the dSph galaxy region to the area of the field region and

$$N_{off}^{UL\,84} \approx (N_{off} + 1)\left[1 - \frac{1}{9(N_{off}+1)} + \frac{1.000}{3\sqrt{N_{off}+1}}\right]^3 \tag{5}$$

The equations are taken from the Appendix of Hughes & Wallerstein (2000), and corresponding to eq. [2] of Mighell et al. (1998) and eq. [9] of Gehrels (1986). Here, Equation 5 is the estimated upper (84%) confidence limit of N_{off}, using Gaussian statistics.

$$N_{on}^{LL\,95} \approx N_{on} \times \left[1 - \frac{1}{9N_{on}} - \frac{1.645}{3\sqrt{N_{on}}} + 0.031N_{on}^{-2.50}\right]^3 \tag{6}$$

The above quantity is then the lower 95% confidence limit for N_{on} (eq. [3] of Mighell et al. 1998, and eq. [14] of Gehrels 1986). The field area was the same as the galaxy area in this case. Then, in

[2]http://stev.oapd.inaf.it/cgi-bin/cmd

order to decide if any particular star is a cluster member, we generate a uniform random number, $0 < p' < 1$. If $p > p'$, we accept the star as a member of the dSph. We ran the cleaning process twice, using the real off-galaxy field for the RGB stars, and then using the TRILEGAL-generated objects for the whole sample. We found that the results were consistent for the overalapping RGB stars.

When the above process is performed for a globular cluster field with thousands (or tens of thousands) of stars, compared with a few hundred non-members, the statistical cleaning process rejects few real cluster members. However, with the small numbers involved here, we are more careful to examine each object (which is also more feasible with 165 objects, rather than thousands). In Table 2, we have identified classes of objects, A–F, which correspond with the likelihood of the object being a real dSph member. Figure 5 is a finding chart for these objects based on the 300s R-image. Table 2 also lists the J2000 equatorial coordinates of the stars, which we derived using the 2MASS stars in the image to construct the plate solution (using the IMCOORDS program suite in IRAF). Objects were ranked as class A if they passed the statistical cleaning process, were in the right color area of Figure 4 (compared with the real off-galaxy field), and had photometry in all filters with uncertainties less than 0.05. A-class objects are shown as filled triangles in Figures 6 & 7. B-class (open triangles) stars passed *cleaning* process but had poorer quality photometry (and are mostly at the MSTO). C-class objects (large open circles) failed the statistical cleaning process at the last stage when they were compared to the random probability, but had the right colors and good photometry. D-class stars (median-sized open circles) failed the statistical cleaning process, have the right colors but poor photometry. E-class stars (small open circles) passed statistical cleaning but failed color-selection, and F-class stars (tiny open circles) failed both statistical cleaning and color-selection.

We compared our RGB stars with the Martin et al. (2007) proper motion survey (see Table 2), and showed that we rejected the non-members in the sample overlap. The only giant which fell outside the A-class was object #8, classified C, which has the right colors, but was in a region of the CMD with many foreground stars. We have shown that the statistical rejection method used alone is unlikely to select a non-member, but might reject a few metal-poor RGB stars.

4. Discussion & Conclusions

The $(T_1 - T_2)$ vs. $(C - T_1)$ color-color plot in Figure 6 of the A-class Boötes I stars (plus #8) show that they are of low metallicity (mostly $[Fe/H] \leq -2.0$). The reddening here is very low, and does not affect the color-color plot significantly. Distance modulus errors are more problematic for the CMDs, but the values used: $(m - M)_V = 19.11 \pm 0.08\ mag$ and $E(B - V) = 0.02$, give consistent fits to the isochrones in both the CMDs and the color-color plots. The star with the very red $(T_1 - T_2)$-color is #29 in Table 2. This star sits at the base of the RGB in Figure 3, and is likely to be a foreground dwarf that did not get rejected statistically.

The Geisler, Claria & Minniti (1991) lines of constant $[Fe/H]$ were derived from real RGB stars in globular and open clusters, where the metal-poor stars tend to be α-enhanced. The models of Marigo et al. (2008) calculate colors for MSTO and MS stars, but are solar-scaled. If we plotted the whole Z=0.0002 model in Figure 6, the MSTO would form a loop beneath the Geisler, Claria & Minniti (1991) grid, and the MS would cross the grid again, close to the locus of the RGB. We have MSTO stars in our data set, but the observations did not sample the MS stars. Any MS stars present on the color-color plots have to be metal-poor halo dwarfs. Since the error bars are relatively large compared to the spacing of the $[Fe/H]$-grid, we use the weighted mean of the [Fe/H]-values for the 7 brightest Boötes I members (filled squares), $[Fe/H] = -2.1^{+0.3}_{-0.5}$. The range looks to be from $-3.5 \leq [Fe/H] \leq -1.8$, for these 7 RGB stars. The metal-rich Boötes I members appear to terminate at about -1.8, but the the metal-poor stars may have lower values than [Fe/H]=-2.5. The Washington filter system becomes less sensitive to $[Fe/H]$ as the metals go to zero (see Figure 2b, where the fiducial RGBs get closer together in $(C - T_1)$ as $[Fe/H]$ reduces), so small errors in color can lead to large errors in $[Fe/H]$.

Our result is consistent with recently reported spectroscopy (Norris et al. 2008; Ivans et al. 2008). Norris et al. (2008) used the AAOmega multifibre facility on the Anglo-Australian Telescope, obtaining spectra over 3800–4600 Å. They used the Ca II K line and the G-band to determine $[Fe/H] = -2.6 \pm 0.5$ for 19 stars, which had S/N > 14 per 0.34 Å pixel at 4100 Å. Ivans et al. (2008) used Magellan's multi-object echellette at Las Campanas Observatory to obtain higher resolution spectra of two Boötes I RGB stars, which were $[Fe/H] = -2.3$ (with $[\alpha/Fe] = +0.4$) and -1.9 ($[\alpha/Fe] = +0.2$). Considering the Salaris et al. (1993) formula for comparing solar-scaled to alpha-enhanced isochrones, $Z = Z_0(0.638 f_\alpha + 0.362)$, where Z_0 is the non-enhanced metallicity and f_α is the average enhancement factor, the RGB in Figure 7a would then appear to be ≥ 0.0001 more metal-rich than is implied by Figure 6 (and the spectroscopic results).

We use the CMD and the color-color plot to estimate the metallicities of the stars, which both have their biasses. Figure 7a shows the CMD for the classes of objects from Table 2. We note that the reddest RGB-tip star is also in the region with many foreground objects, whereas the MSTO stars are relatively uncontaminated. The star (#8) which is close to the horizontal branch area was not noted as variable in Siegel (2006) and looks to be more metal rich that the rest of the class A stars, but is not inconsistent with the spectroscopic data, discussed previously. The base of the RGB is also an area which had many foreground contaminants. The relatively-clean MSTO region shows a tight, single turn-off, which can be reproduced by the main Boötes I stars having Z=0.0002 and an age of 14.1 Gyrs, with some stars being as metal-rich as Z=0.0003 at 12.2 Gyrs. We show that these isochrones (Marigo et al. 2008)[3] overlap, giving a narrow MSTO-SGB region, and are

[3]These new isochrones are solar-scaled, but there has been considerable discussion in recent papers (see Bertelli et al. 2008; VandenBerg et al. 2007) on whether the new lower solar abundances (Asplund et al. 2005; 2006) are inconsistent with helioseismology. Bertelli et al. use Z=0.017 for the sun, which they acknowledge is a compromise between the usual value of $Z \approx 0.02$ and the lower values derived by Asplund et al. (2005; 2006), but matches the accepted $R_\odot$, $L_\odot$ to within 0.2% and R_c to about 1%.

consistent with the color-color plot in Figure 6.

We note the presence of at least 4 blue straggler stars (BSS), which passed the cleaning process and are well-separated from the other MSTO stars in $(T_1 - T_2)$ and. $(C - T_1)$. We show the isochrones for the most metal-poor models (Z=0.0001) for 4.5 & 0.004 Gyr. The bluest BSS seem to be on the metal-poor main sequence, which appears to be more metal-poor than Z=0.0001. BSS are either *primordial* (having been formed with the rest of the stellar population in the system) or *collisional* (formed at different epochs due to collisions or close passes between stars). Momany et al. (2007) discussed the BSS population of dSphs that had not undergone recent star formation, which included Boötes I. They found that the BSS frequency for the lowest luminosity dwarf galaxies (which again includes Boötes I) agreed with the frequency for the Milky Way halo and open clusters; and they derived a statistically significant $F_{HB}^{BSS} - M_V$ anti-correlation for these dSphs similar to that observed in globular clusters. Figure 7 does show the suggestion of a *blue plume,* which is an old BSS population (similar to that seen in open and globular clusters in our galaxy), but the photometric errors are larger, and the color-separation is less clear. In the A-class sample of Table 2, there is one possible HB star and at least 4 BSS, making the Momany et al. (2007) statistic $F_{HB}^{BSS} = log(N_{BSS}/N_{HB}) = 0.6$, for this central region, whereas Momany et al. (2007) find it is ~ 0.25 for the whole Boötes I field. The known RR Lyrae stars are outside our central field, but the central Boötes I population has its F_{HB}^{BSS}-value closer to the mean BBS values for the Milky Way halo (Preston & Sneden 2000). Ferraro et al. (2006) analyzed the BS population of ω Cen (a non-relaxed system), deciding that the stars had to be produced by non-collisional processes. Certainly, in this sparsely populated dSph, these BS also have to be non-collisional in origin. There is no evidence of recent star formation in Boötes I, with Bailin & Ford (2007) finding it devoid of HI gas.

Unlike the previously-published photometry in BVI (Siegel 2006; Dall'Ora et al. 2006) and gi (B06), the MSTO region is clearly separated from the foreground stars in the Washington filters. Zucker et al. (2006b) saw clear evidence for a broadened MSTO and SGB in the UMa II Dwarf, and while there is likely some spread in [Fe/H] at the MSTO, the distribution of MSTO and SGB stars argues against a long period of continuous star formation (more than about 2 Gyr), and a ≥ 1.0 dex spread in $[Fe/H]$. Membership can be more properly determined by radial velocity studies, such as that by Muñoz et al. (2006) and Martin et al. (2007), but these can only be performed on large telescopes for giants. In the Muñoz et al. (2006) study (discussed in §1), 58 stars were observed, selected as having the correct colors (in the gi-filters) to be RGB or AGB objects belonging to Boötes I. Only 12 objects had radial velocities in the expected range (95.6 ± 3.4 km/s), with only 7 being within the half-light radius , showing the need for having a better method of preselecting RGB candidates before committing to spectroscopy. Our CT_1T_2 photometry shows a narrow MSTO and SGB, with a metallicity of $[Fe/H] = -2.1^{+0.3}_{-0.5}$ for the RGB and MSTO, with ages ranging from 12–14 Gyr, using the new Marigo et al. (2008) isochrones. In this study, Boötes I appears to be similar to, or slightly more metal poor than, M15, but does appear to have a small metallicity spread.

The authors wish to thank Ata Sarajedini and Doug Geisler for sharing their data, Ivan King for advice. This paper used observations obtained with the Apache Point Observatory 3.5-meter telescope, which is owned and operated by the Astrophysical Research Consortium. Hughes is grateful for all the help provided by the APO telescope operators during remote observing. We also acknowledge support from the Kennilworth Fund, of the New York Community Trust. Anne Bossi acknowledges support from the Washington NASA Space Grant Consortium and the Welch family. We also thank Leo Girardi for providing the web interface for his isochrones and the TRILEGAL 1.1 code, and an anonymous referee for improving the paper.

REFERENCES

Asplund, M., Grevesse, N., Sauval, A.J., Allende Prieto, C., Blomme, R. 2005, A&A, 431,693

Asplund, M., Grevesse, N., Sauval, A.J. 2006, Comm. in Asteroseismology, Vol. 147, p.76

Bailin, J., & Ford, A., 2007, MNRAS, 375, L41.

Belokurov, V. et al. 2006a, ApJ, 647, L111

Belokurov, V. et al. 2006b, ApJ, 642, L137

Bertelli, G., Girardi, L., Marigo, P., Nasi, E. 2008, A&A, 484, 815

Dall'Ora, M., Clementini, G., Kinemuchi, K., Ripepi, V., Marconi, M., Di Fabrizio, L., Greco, C., Rodgers, C. T., Kuehn, C., & Smith, H. A. 2006, ApJ, 653, L109

de Jong, J. T. A., Rix, H.-W., Martin, N. F., Zucker, D. B., Dolphin, A. E., Bell, E. F., Belokurov, V., & Evans, N. W. 2008, AJ, 135, 1361

Ferraro, F.R., Sollima, A., Rood, R.T., Origlia, L., Pancino, E., & Bellazzini, M. 2006, ApJ, 638, 433

Gehrels, N. 1986, ApJ, 303, 336

Geisler, G. 1996, AJ, 111, 480

Geisler, D., Claria, J.J., & Minniti, D. 1991, AJ, 102, 1836

Geisler, D., & Sarajedini, A. 1999, AJ, 117, 308

Girardi, L., Groenewegen, M. A. T., Hatziminaoglou, E., & da Costa, L. 2005, A&A, 436, 895

Hughes, J., & Wallerstein, G. 2000, AJ, 119, 1225

Hughes, J., Wallerstein, G., Covarrubias, R., & Hays, N. 2007, AJ, 134, 229

Ivans, I., et al. 2008, in preparation.

Marigo, P., Girardi, L., Bressan, A., Groenewegen, M. A. T., Silva, L., & Granato, G. L. 2008, A&A, 482, 833

Martin, N. F., Ibata, R. A., Chapman, S. C., Irwin, M. & Lewis, G. F. 2007, MNRAS, 380, 281

Mighell, K.J., Sarajedini, A., & French, R.S. 1998, AJ, 116, 2395

Momany, Y., Held, E. V., Saviane, I., Zaggia, S., Rizzi, L., & Gullieuszik, M. 2007, A&A, 468, 973

Muñoz, R. R., Carlin, J. L., Frinchaboy, P. M., Nidever, D. L., Majewski, S. R., & Patterson, R. J. 2006, ApJ, 650, L51

Norris, J.E., Gilmore, G., & Wyse, R.F.G. 2008, in preparation.

Preston, G. W., & Sneden, C. 2000, AJ, 120, 1014

Salaris, M., Chieffi, A., & Straniero, O. 1993, ApJ, 414, 580

Siegel, M. H. 2006, ApJ, 649, L83

Siegel, M. H., Shetrone, M.D, & Irwin, M. 2008, AJ, 135, 2084

Stetson, P.B., Davis, L.E., & Crabtree, D.R. 1990, ASPC, 8, 289

Vandenberg, D., A., Edvardsson, B., Eriksson, K., Gustafsson, B.., Ferguson, J. W. 2007, ApJ, 666, L105

Twarog, B.A., Corder, S., & Anthong-Twarog, B.J. 2006, AJ, 132, 299

Walsh, S., Jerjen, H., Willman, B. 2007, ApJ, 662, L83

Willman, B., et al. 2005a, AJ, 129, 2692

Willman, B., et al. 2005b, ApJ, 626, L85

York D.G., et al. 2000, AJ, 120, 1579

Zinn, R. 1985, ApJ, 293, 424

Zucker, D. B., et al. 2006a, ApJ, 643, L103

Zucker, D. B., et al. 2006b, ApJ, 650, L41

Figure Captions

Fig.1:- Plot of the final uncertainties (calculated from the ALLSTAR uncertainty, aperture correction, and the standard-star photometry, taken in quadrature) of the sources in Table 2. From the DAOPHOT-ALLSTAR output, we selected objects with a CHI-value (the DAOPHOT goodness-of-fit statistic) between 0.5 and 1.5. **(a)** The σ_{T_1}-value versus the T_1 magnitude.
(b) The uncertainty versus T_1 magnitude for $(C - T_1)$.
(c) The uncertainty versus T_1 magnitude for $(T_1 - T_2)$.

Fig.2:- (a) T_1 vs. $(C - T_1)$ CMD of the 165 stars detected in the Boötes I field, uncorrected for distance or extinction, shown as open squares with error bars.
(b) M_{T_1} vs. $(C - T_1)$ CMD of the stars in the Boötes I field. The small circles are M15 data from GS99. The open squares with error bars are the 165 objects from Table 2, shown with the standard giant branches from GS99. We use the distance modulus of 19.11 and $E(B - V) = 0.02$ for Boötes I, with $(m - M)_V = 15.41$ and $E(B - V) = 0.10$ for M15.

Fig.3:- M_{T_1} vs. $(C - T_1)$ CMD of the stars in the Boötes I field. The small circles are M15 data from GS99, the open squares are the 165 objects from Table 2, the open stars are foreground stars from a nearby field, the crosses are a simulated stellar population using the TRILEGAL code (Girardi et al. 2005), using the same area and limiting magnitude. We plot the Z=0.0002, 14.1 Gyr, and Z=0.0006, 12.7 Gyr isochrones (Marigo et al. 2008) for comparison. For Boötes I, we use $(m - M)_V = 19.11$ and $E(B - V) = 0.02$.

Fig.4:- $(T_1 - T_2)$ vs. $(C - T_1)$ color-color plot of the Boötes I stars with uncertainties better than 0.05, shown as filled squares. The constant-$[Fe/H]$ lines from Geisler, Claria & Minniti (1991) are marked. The Z=0.0006, 12.7 Gyr, isochrone of Marigo et al. (2008) is shown from the MSTO to the tip of the RGB. Again, the open stars are foreground stars from a nearby field, the crosses are a simulated stellar population using the TRILEGAL code (Girardi et al. 2005), using the same area and limiting magnitude.

Fig.5:- The 300s R-band image of a field of the Boötes I dwarf galaxy, taken with the APO 3.5-m telescope and SPIcam (north is up, east is left. FOV$\sim 4.78' \times 4.78'$). The numbers correspond to the sources in Table 2, with the plate solutions from the 2MASS catalog to convert the xy-coordinates to right ascension and declination (J2000).

Fig.6:- $(T_1 - T_2)$ vs. $(C - T_1)$ color-color plot of the Boötes I stars with uncertainties better than 0.05 in all filters and designated class A (and #8, a C-class, radial velocity member) in Table 2, shown as filled triangles. Star #19 is too red in $(T_1 - T_2)$, and might be two unresolved stars. The constant-$[Fe/H]$ lines for RGB stars from Geisler, Claria & Minniti (1991) are marked. The Z=0.0001, 0.0002, and 0.0003, 12.7 Gyr, isochrones of Marigo et al. (2008) are plotted from the MSTO to the tip of the RGB. We note that all the isochrones from 10-15 Gyr fall almost on top of each other on this color-color plot, since these colors are only sensitive to metallicity, not age. The 7 brightest cluster members are shown as filled squares.

Fig.7:- (a) CMD for Boötes I stars. Filled triangles are class A, open triangles are class B, the classes C-F are decreasing sizes of open circles. For the filled triangles, the error bars are the same size as the points. We show various isochrones from Marigo et al. (2008), including those close to the possible blue stragglers.
(b) MSTO-SGB region of the CMD for Boötes I stars. Class A objects (filled triangles) have error bars, which are much larger on the other points and are not shown (class B, open triangles, are shown for their general trend). We show the isochrones from Marigo et al. (2008).

Table 1. APO 3.5-m CCD Frames taken in Spring 2007

Field	Filter	Exposure(s)	Airmass[1]	FWHM(arcsec)[2]
Boötes I[3]	R	1	1.069	0.9
Boötes I	R	3	1.067	0.8
Boötes I	R	10	1.065	0.8
Boötes I	R	30	1.064	0.8
Boötes I	R	90	1.063	0.8
Boötes I	R	300	1.060	0.7
Boötes I	R	1000	1.058	0.8
Boötes I	I	1	1.054	0.6
Boötes I	I	3	1.053	0.6
Boötes I	I	10	1.053	0.6
Boötes I	I	30	1.053	0.6
Boötes I	I	90	1.053	0.7
Boötes I	I	300	1.053	0.7
Boötes I	I	1000	1.054	0.8
Boötes I	C	1	1.060	0.7
Boötes I	C	3	1.061	0.9
Boötes I	C	10	1.062	0.8
Boötes I	C	30	1.063	0.7
Boötes I	C	90	1.065	0.8
Boötes I	C	300	1.068	0.7
Boötes I	C	1000	1.072	0.7

Note. — (1) Effective airmass. (2) Average seeing. (3) 2007 March 19.

Table 2. Sample of Objects in Bootes I Central Field

ID	X_C	Y_C	T_1	σ_{T_1}	C	σ_C	T_2	σ_{T_2}	RA	Dec	Type	Note
1	465.650	672.994	11.364	0.011	12.868	0.034	10.900	0.018	14:00:07.26	14:30:44.2	F	2MASS 14000725+1430443
2	404.362	408.282	14.334	0.011	15.575	0.027	13.957	0.018	14:00:08.43	14:29:29.8	F	2MASS 14000844+1429296
3	960.096	499.425	16.011	0.012	19.482	0.030	14.356	0.022	13:59:57.69	14:29:55.6	F	2MASS 13595769+1429554, VR
4	54.569	53.073	16.241	0.011	19.528	0.033	14.960	0.026	14:00:15.18	14:27:49.8	F	2MASS 14001516+1427499
5	308.687	801.328	16.690	0.011	18.336	0.027	16.158	0.018	14:00:10.30	14:31:20.2	F	2MASS 14001029+1431205
6	630.807	818.253	16.863	0.011	18.065	0.026	16.378	0.018	14:00:04.07	14:31:25.1	E	2MASS 14000406+1431251
7	962.627	499.406	17.166	0.014	21.172	0.061	15.259	0.023	13:59:57.64	14:29:55.6	E	···
8	298.684	891.947	17.224	0.013	19.050	0.026	16.612	0.018	14:00:10.49	14:31:45.6	C	2MASS 14001049+1431454, VA
9	330.672	171.268	17.507	0.011	19.300	0.028	16.933	0.017	14:00:09.85	14:28:23.1	A	2MASS 14000985+1428228
10	15.427	605.009	17.642	0.011	18.430	0.030	17.292	0.017	14:00:15.96	14:30:24.9	F	···
11	891.801	840.981	17.712	0.012	20.972	0.028	16.608	0.017	13:59:59.02	14:31:31.5	E	2MASS 13595900+1431317
12	480.032	970.838	17.771	0.011	19.350	0.026	17.305	0.017	14:00:06.99	14:32:07.9	E	VR
13	207.843	915.000	18.007	0.011	18.915	0.029	17.618	0.017	14:00:12.25	14:31:52.1	F	2MASS 14001226+1431518, VR
14	540.963	301.431	18.626	0.012	19.588	0.029	18.230	0.017	14:00:05.78	14:28:59.8	E	···
15	461.309	912.008	18.794	0.011	22.179	0.033	17.496	0.017	14:00:07.35	14:31:51.3	E	2MASS 14000735+1431511, VR
16	287.259	389.960	18.919	0.011	20.289	0.027	18.401	0.017	14:00:10.69	14:29:24.6	A	···
17	72.984	337.386	19.056	0.012	19.932	0.029	18.675	0.018	14:00:14.84	14:29:09.7	F	···
18	171.206	684.411	19.228	0.012	21.339	0.029	18.639	0.017	14:00:12.95	14:30:47.3	E	···
19	626.801	6.284	19.329	0.017	20.196	0.030	18.953	0.018	14:00:04.11	14:27:36.9	A	Not RR Lyrae?
20	329.809	701.761	19.370	0.011	22.101	0.031	18.513	0.017	14:00:09.88	14:30:52.2	E	VR
21	963.849	2.411	19.567	0.013	22.689	0.057	18.628	0.019	13:59:57.59	14:27:35.9	E	···
22	950.939	97.894	19.776	0.012	20.970	0.035	19.302	0.019	13:59:57.85	14:28:02.8	A	···
23	496.407	265.649	19.815	0.012	23.596	0.054	18.215	0.017	14:00:06.64	14:28:49.7	E	···
24	667.937	272.143	20.127	0.013	21.189	0.029	19.626	0.018	14:00:03.33	14:28:51.6	C	···
25	5.815	897.782	20.210	0.012	21.179	0.034	19.836	0.020	14:00:16.16	14:31:47.1	F	···
26	589.614	886.856	20.301	0.016	23.082	0.042	19.417	0.018	14:00:04.87	14:31:44.3	E	VR
27	602.727	828.935	20.427	0.013	24.009	0.056	18.719	0.018	14:00:04.61	14:31:28.1	E	VR
28	564.802	599.216	20.472	0.014	21.576	0.033	19.968	0.021	14:00:05.34	14:30:23.5	A	···
29	510.876	714.457	20.473	0.015	21.672	0.030	19.844	0.022	14:00:06.38	14:30:55.8	A	···
30	672.201	367.862	20.570	0.013	24.163	0.113	19.064	0.018	14:00:03.25	14:29:18.5	E	···
31	207.935	381.417	20.722	0.015	21.696	0.030	20.265	0.021	14:00:12.23	14:29:22.1	C	···
32	692.683	332.819	20.775	0.012	21.539	0.031	20.414	0.020	14:00:02.85	14:29:08.7	E	···
33	848.414	14.943	20.845	0.014	21.808	0.038	20.481	0.025	13:59:59.83	14:27:39.4	E	Close to V8
34	681.498	600.224	20.870	0.014	21.992	0.038	20.407	0.020	14:00:03.08	14:30:23.8	A	VA
35	716.246	951.889	20.894	0.021	23.482	0.054	20.188	0.021	14:00:02.42	14:32:02.6	E	···

Table 2—Continued

ID	X_C	Y_C	T_1	σ_{T_1}	C	σ_C	T_2	σ_{T_2}	RA	Dec	Type	Note
36	653.274	903.421	20.954	0.016	22.070	0.041	20.546	0.020	14:00:03.64	14:31:49.0	E	···
37	925.807	867.628	21.055	0.014	22.859	0.044	20.465	0.020	13:59:58.36	14:31:39.0	E	···
38	711.904	758.333	21.081	0.061	23.262	0.084	20.340	0.050	14:00:02.50	14:31:08.3	F	···
39	664.767	875.856	21.264	0.016	23.105	0.044	20.655	0.024	14:00:03.41	14:31:41.3	F	···
40	789.328	824.543	21.285	0.017	22.411	0.035	20.780	0.025	14:00:01.00	14:31:26.9	A	···
41	641.611	905.460	21.377	0.055	23.642	0.085	20.705	0.053	14:00:03.86	14:31:49.6	E	···
42	917.939	724.559	21.486	0.014	22.618	0.035	21.083	0.038	13:59:58.51	14:30:58.8	C	···
43	6.632	97.070	21.507	0.016	22.604	0.052	21.216	0.034	14:00:16.11	14:28:02.1	E	···
44	945.510	434.384	21.521	0.019	22.518	0.035	21.128	0.024	13:59:57.97	14:29:37.3	E	···
45	545.050	475.098	21.539	0.015	21.745	0.031	20.970	0.031	14:00:05.71	14:29:48.6	A	BSS
46	452.631	123.614	21.728	0.021	23.565	0.060	21.142	0.023	14:00:07.48	14:28:09.8	E	···
47	673.778	935.680	21.751	0.023	22.669	0.037	21.282	0.032	14:00:03.24	14:31:58.1	A	···
48	845.796	760.066	21.817	0.019	21.733	0.033	21.650	0.042	13:59:59.91	14:31:08.8	A	BSS
49	361.348	389.829	21.832	0.016	24.245	0.087	20.416	0.019	14:00:09.26	14:29:24.6	E	···
50	87.948	538.212	21.915	0.019	22.771	0.041	21.513	0.028	14:00:14.56	14:30:06.1	A	···
51	661.843	801.672	21.921	0.023	22.252	0.035	21.640	0.043	14:00:03.47	14:31:20.4	A	BSS
52	137.089	649.530	21.940	0.023	22.829	0.040	21.519	0.040	14:00:13.61	14:30:37.4	A	···
53	977.369	783.827	21.946	0.022	22.597	0.042	21.529	0.057	13:59:57.36	14:31:15.5	B	···
54	148.239	789.076	21.971	0.022	22.848	0.042	21.504	0.048	14:00:13.40	14:31:16.7	A	···
55	218.112	626.465	21.980	0.084	25.480	0.295	20.289	0.019	14:00:12.04	14:30:31.0	E	···
56	957.905	376.235	21.982	0.025	22.820	0.041	21.660	0.055	13:59:57.72	14:29:21.0	B	···
57	138.957	212.847	22.045	0.031	22.464	0.053	21.844	0.044	14:00:13.55	14:28:34.7	B	BSS
58	908.028	210.687	22.047	0.075	24.180	0.342	21.442	0.040	13:59:58.68	14:28:34.4	F	···
59	189.245	603.444	22.064	0.022	22.705	0.059	21.781	0.052	14:00:12.60	14:30:24.5	E	···
60	676.467	342.658	22.066	0.018	22.843	0.042	21.635	0.058	14:00:03.16	14:29:11.4	B	···
61	957.068	756.913	22.067	0.023	22.912	0.041	21.595	0.039	13:59:57.75	14:31:07.9	A	···
62	979.011	569.678	22.096	0.016	22.912	0.041	21.832	0.055	13:59:57.32	14:30:15.3	E	···
63	619.808	1012.61	22.144	0.017	22.848	0.044	21.821	0.035	14:00:04.29	14:32:19.7	A	···
64	536.738	928.120	22.146	0.028	22.898	0.039	21.678	0.048	14:00:05.89	14:31:55.9	A	···
65	974.000	568.127	22.195	0.026	22.913	0.049	21.987	0.042	13:59:57.42	14:30:14.9	F	···
66	33.712	77.835	22.197	0.042	22.988	0.050	21.614	0.038	14:00:15.58	14:27:56.8	B	···
67	341.736	365.060	22.201	0.025	22.283	0.035	22.227	0.048	14:00:09.64	14:29:17.6	A	···
68	952.338	152.183	22.226	0.024	22.700	0.044	22.098	0.080	13:59:57.82	14:28:18.0	B	···
69	956.856	124.497	22.278	0.029	23.263	0.048	21.875	0.065	13:59:57.73	14:28:10.2	E	···
70	426.090	967.923	22.334	0.039	23.146	0.047	21.927	0.033	14:00:08.03	14:32:07.0	A	···

Table 2—Continued

ID	X_C	Y_C	T_1	σ_{T_1}	C	σ_C	T_2	σ_{T_2}	RA	Dec	Type	Note
71	810.443	896.079	22.334	0.028	23.113	0.043	21.722	0.061	14:00:00.60	14:31:47.0	B	···
72	882.343	409.180	22.342	0.019	23.079	0.050	21.953	0.037	13:59:59.19	14:29:30.2	B	···
73	148.738	278.495	22.381	0.026	23.923	0.109	21.713	0.038	14:00:13.37	14:28:53.2	E	···
74	253.582	998.234	22.395	0.021	23.613	0.058	21.939	0.042	14:00:11.37	14:32:15.5	E	···
75	958.295	953.537	22.407	0.025	23.169	0.056	22.136	0.079	13:59:57.74	14:32:03.2	B	···
76	77.620	796.977	22.409	0.019	23.252	0.050	22.353	0.048	14:00:14.77	14:31:18.9	E	···
77	820.070	745.891	22.426	0.052	22.975	0.044	22.008	0.053	14:00:00.40	14:31:04.8	B	···
78	150.535	411.135	22.449	0.026	23.113	0.047	22.252	0.075	14:00:13.34	14:29:30.5	E	···
79	57.414	71.384	22.477	0.020	23.350	0.071	21.924	0.051	14:00:15.13	14:27:55.0	E	···
80	587.436	178.073	22.481	0.035	23.009	0.047	22.044	0.064	14:00:04.88	14:28:25.2	B	···
81	372.655	921.741	22.496	0.019	23.161	0.051	22.293	0.108	14:00:09.07	14:31:54.0	B	···
82	313.526	867.753	22.515	0.019	23.258	0.054	22.298	0.090	14:00:10.21	14:31:38.8	B	···
83	243.621	710.867	22.519	0.032	23.243	0.056	22.403	0.066	14:00:11.55	14:30:54.7	E	···
84	334.968	513.434	22.523	0.028	23.079	0.054	22.062	0.053	14:00:09.78	14:29:59.3	B	···
85	226.373	789.191	22.553	0.035	23.252	0.049	22.282	0.048	14:00:11.89	14:31:16.7	A	···
86	77.601	787.030	22.566	0.022	23.308	0.052	22.236	0.042	14:00:14.77	14:31:16.1	B	···
87	406.006	57.568	22.588	0.029	23.212	0.054	22.363	0.050	14:00:08.38	14:27:51.2	E	···
88	858.335	565.959	22.592	0.031	23.185	0.055	22.247	0.101	13:59:59.66	14:30:14.3	B	···
89	613.419	448.395	22.601	0.030	23.063	0.064	22.277	0.075	14:00:04.39	14:29:41.1	D	···
90	201.889	449.136	22.605	0.038	22.984	0.047	22.599	0.054	14:00:12.35	14:29:41.2	B	···
91	385.872	256.560	22.638	0.039	23.085	0.047	22.202	0.060	14:00:08.78	14:28:47.1	B	···
92	324.001	760.919	22.650	0.023	23.456	0.067	22.245	0.075	14:00:10.00	14:31:08.8	B	···
93	753.361	54.971	22.656	0.037	23.434	0.062	22.282	0.101	14:00:01.67	14:27:50.6	B	···
94	610.504	506.923	22.670	0.021	23.225	0.054	22.466	0.091	14:00:04.45	14:29:57.6	E	···
95	280.485	123.461	22.675	0.025	23.360	0.050	22.236	0.047	14:00:10.81	14:28:09.7	B	···
96	483.257	776.163	22.675	0.029	23.969	0.092	21.783	0.036	14:00:06.92	14:31:13.2	E	···
97	760.545	325.963	22.699	0.026	23.756	0.084	21.869	0.035	14:00:01.54	14:29:06.8	E	···
98	311.522	242.684	22.699	0.024	23.178	0.050	22.416	0.065	14:00:10.22	14:28:43.2	B	···
99	492.600	869.320	22.721	0.022	23.405	0.092	22.468	0.075	14:00:06.74	14:31:39.4	B	···
100	182.199	285.789	22.734	0.033	23.554	0.058	22.371	0.057	14:00:12.72	14:28:55.3	E	···
101	239.042	3.639	22.743	0.045	23.467	0.058	22.882	0.142	14:00:11.61	14:27:36.0	E	···
102	952.695	130.212	22.757	0.038	23.439	0.052	22.287	0.048	13:59:57.81	14:28:11.8	B	···
103	943.911	485.903	22.773	0.035	23.733	0.079	21.413	0.103	13:59:58.00	14:29:51.8	E	···
104	878.449	266.052	22.785	0.031	23.670	0.154	22.100	0.059	13:59:59.26	14:28:50.0	B	···
105	480.903	322.344	22.792	0.024	23.464	0.061	22.571	0.091	14:00:06.95	14:29:05.6	B	···

Table 2—Continued

ID	X_C	Y_C	T_1	σ_{T_1}	C	σ_C	T_2	σ_{T_2}	RA	Dec	Type	Note
106	420.243	500.004	22.797	0.047	23.343	0.076	22.638	0.135	14:00:08.13	14:29:55.5	B	···
107	694.793	586.227	22.805	0.042	23.360	0.067	22.288	0.052	14:00:02.82	14:30:19.9	B	···
108	40.007	597.012	22.810	0.041	23.408	0.100	22.413	0.109	14:00:15.49	14:30:22.6	B	···
109	343.575	849.542	22.811	0.028	23.425	0.058	22.395	0.054	14:00:09.62	14:31:33.7	B	···
110	641.122	456.282	22.813	0.040	23.219	0.064	22.413	0.045	14:00:03.85	14:29:43.3	B	···
111	279.935	508.314	22.814	0.031	23.953	0.104	21.846	0.034	14:00:10.84	14:29:57.8	E	···
112	908.838	495.568	22.816	0.048	23.313	0.051	22.252	0.073	13:59:58.68	14:29:54.5	B	···
113	402.070	893.008	22.828	0.042	23.504	0.062	22.386	0.078	14:00:08.50	14:31:46.0	B	···
114	716.162	994.159	22.846	0.040	23.794	0.076	22.341	0.089	14:00:02.42	14:32:14.5	E	···
115	121.874	698.918	22.850	0.043	23.437	0.062	22.312	0.084	14:00:13.91	14:30:51.3	B	···
116	836.493	275.678	22.853	0.039	23.410	0.055	22.784	0.126	14:00:00.07	14:28:52.7	E	···
117	599.412	853.925	22.866	0.025	23.445	0.058	22.944	0.135	14:00:04.68	14:31:35.1	E	···
118	738.943	659.646	22.873	0.053	23.457	0.080	22.592	0.091	14:00:01.97	14:30:40.5	B	···
119	558.704	834.797	22.875	0.025	23.414	0.068	22.514	0.056	14:00:05.46	14:31:29.7	B	···
120	411.578	218.014	22.879	0.040	23.488	0.080	22.579	0.116	14:00:08.28	14:28:36.3	B	···
121	505.004	301.975	22.912	0.042	23.649	0.072	22.387	0.099	14:00:06.48	14:28:59.9	B	···
122	179.055	455.900	22.926	0.026	23.641	0.097	22.580	0.090	14:00:12.79	14:29:43.1	B	···
123	730.465	611.611	22.927	0.027	23.572	0.077	22.460	0.100	14:00:02.13	14:30:27.0	B	···
124	862.889	929.290	22.928	0.045	23.558	0.053	22.729	0.069	13:59:59.58	14:31:56.3	E	···
125	608.254	752.400	22.957	0.053	23.729	0.083	22.343	0.083	14:00:04.50	14:31:06.5	B	···
126	786.331	979.146	22.961	0.047	23.785	0.071	22.465	0.094	14:00:01.07	14:32:10.3	B	···
127	953.222	991.316	22.976	0.042	23.819	0.073	22.445	0.064	13:59:57.84	14:32:13.8	B	···
128	665.141	568.773	22.985	0.049	23.724	0.074	22.997	0.095	14:00:03.39	14:30:15.0	E	···
129	963.374	829.092	23.017	0.062	23.879	0.072	23.113	0.107	13:59:57.63	14:31:28.2	E	···
130	807.932	279.447	23.025	0.060	23.526	0.061	22.511	0.082	14:00:00.62	14:28:53.7	B	···
131	399.059	356.671	23.038	0.028	23.594	0.072	22.509	0.122	14:00:08.53	14:29:15.3	B	···
132	898.085	163.200	23.051	0.067	23.651	0.074	22.476	0.054	13:59:58.87	14:28:21.1	B	···
133	967.446	717.057	23.074	0.038	23.484	0.077	22.334	0.059	13:59:57.55	14:30:56.7	B	···
134	229.554	516.635	23.079	0.027	23.796	0.093	22.512	0.094	14:00:11.82	14:30:00.1	B	···
135	728.910	249.357	23.081	0.085	23.810	0.103	22.449	0.112	14:00:02.15	14:28:45.2	B	···
136	532.350	73.423	23.095	0.052	23.696	0.075	22.636	0.092	14:00:05.94	14:27:55.7	B	···
137	777.719	982.319	23.121	0.033	23.878	0.097	22.588	0.067	14:00:01.23	14:32:11.2	B	···
138	577.228	1009.81	23.132	0.050	23.801	0.081	22.728	0.074	14:00:05.11	14:32:18.9	B	···
139	505.335	239.159	23.190	0.057	23.787	0.086	22.752	0.080	14:00:06.47	14:28:42.3	B	···
140	895.176	649.082	23.198	0.069	23.667	0.070	23.163	0.116	13:59:58.95	14:30:37.6	B	···

Table 2—Continued

ID	X_C	Y_C	T_1	σ_{T_1}	C	σ_C	T_2	σ_{T_2}	RA	Dec	Type	Note
141	498.063	375.604	23.235	0.080	23.812	0.092	22.920	0.142	14:00:06.62	14:29:20.6	B	···
142	10.353	402.258	23.242	0.060	23.957	0.077	22.582	0.134	14:00:16.05	14:29:27.9	B	···
143	201.894	479.908	23.266	0.067	23.983	0.107	22.234	0.065	14:00:12.35	14:29:49.8	B	···
144	342.190	368.437	23.277	0.069	23.893	0.111	23.459	0.174	14:00:09.63	14:29:18.5	E	···
145	252.969	910.391	23.281	0.066	23.769	0.073	23.341	0.135	14:00:11.38	14:31:50.8	D	···
146	451.268	822.990	23.296	0.039	23.468	0.070	22.979	0.092	14:00:07.54	14:31:26.3	B	···
147	7.398	1008.48	23.311	0.060	24.098	0.094	23.808	0.247	14:00:16.13	14:32:18.3	E	···
148	905.426	391.313	23.312	0.064	24.045	0.117	22.733	0.136	13:59:58.74	14:29:25.2	B	···
149	678.311	200.695	23.356	0.067	23.672	0.077	23.346	0.133	14:00:03.12	14:28:31.5	B	···
150	718.523	463.654	23.362	0.039	24.077	0.106	22.908	0.129	14:00:02.36	14:29:45.5	B	···
151	828.898	602.344	23.367	0.037	24.145	0.109	22.580	0.059	14:00:00.23	14:30:24.5	B	···
152	199.140	888.963	23.384	0.049	23.989	0.091	23.028	0.100	14:00:12.42	14:31:44.8	D	···
153	26.274	659.335	23.394	0.067	24.001	0.105	22.582	0.066	14:00:15.75	14:30:40.2	B	···
154	404.574	911.300	23.417	0.078	23.990	0.103	23.547	0.161	14:00:08.45	14:31:51.1	E	···
155	697.135	261.617	23.471	0.069	23.926	0.100	22.560	0.065	14:00:02.76	14:28:48.7	B	···
156	582.196	364.987	23.475	0.072	24.125	0.126	23.432	0.141	14:00:04.99	14:29:17.7	E	···
157	377.303	345.663	23.489	0.067	24.127	0.100	23.273	0.121	14:00:08.95	14:29:12.2	B	···
158	311.717	690.271	23.506	0.050	24.219	0.122	23.946	0.296	14:00:10.23	14:30:49.0	E	···
159	657.320	652.457	23.517	0.043	24.127	0.107	22.865	0.089	14:00:03.55	14:30:38.5	B	···
160	237.679	977.635	23.536	0.078	24.366	0.121	22.767	0.082	14:00:11.68	14:32:09.7	B	···
161	688.043	796.889	23.547	0.045	24.144	0.121	22.515	0.134	14:00:02.96	14:31:19.1	B	···
162	522.233	950.515	23.559	0.073	24.287	0.107	22.885	0.109	14:00:06.17	14:32:02.2	B	···
163	270.179	463.211	23.579	0.049	24.265	0.150	22.477	0.056	14:00:11.03	14:29:45.1	B	···
164	471.906	883.595	23.605	0.047	24.321	0.126	23.996	0.240	14:00:07.14	14:31:43.4	E	···
165	576.388	537.281	23.636	0.044	24.085	0.104	23.354	0.134	14:00:05.11	14:30:06.1	B	···

Note. —

A - Sources which have passed statistical cleaning and color-selection, and which have uncertainties better than 0.05 in all filters.

B - Sources which have passed statistical cleaning and color-selection, which do not have uncertainties better than 0.05 in all filters.

C - Sources which passed color-selection failed statistical cleaning, and which have uncertainties better than 0.05 in all filters.

D - Sources which passed color-selection, failed statistical cleaning, and do not have uncertainties better than 0.05 in all filters.

E - Sources which passed statistical cleaning but failed color selection.

F - Sources which failed statistical cleaning and color selection.

VA - Source accepted by Martin et al.'s (2006) radial velocity study.
VR - Source rejected by Martin et al.'s (2006) radial velocity study.
BSS - Possible blue straggler star.

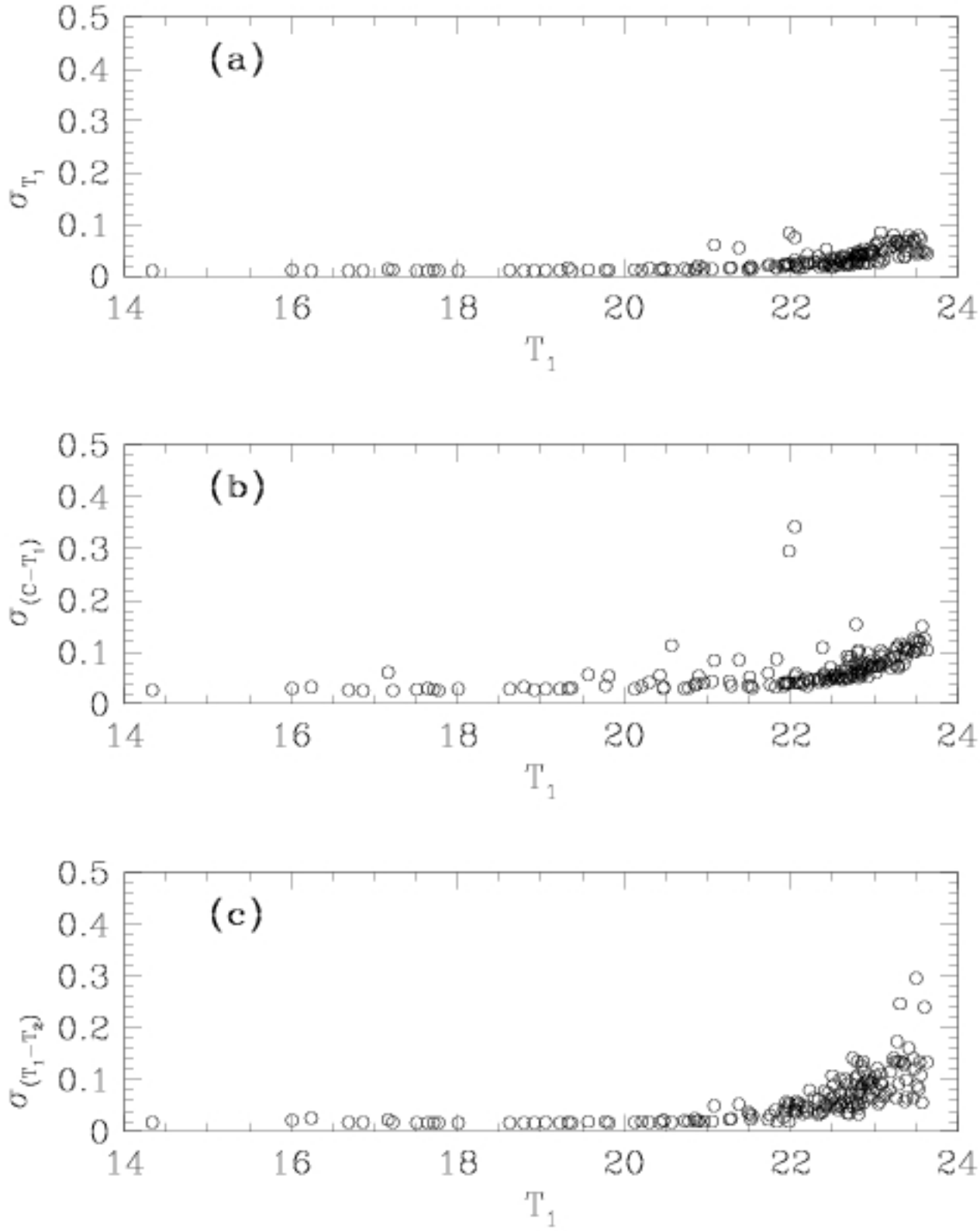
(a)
(b)
(c)
0.5
0.4
0.3
0.2
0.1
0
14
16
18
20
22
24
T_1
σ_{T_1}
$\sigma_{(C-T_1)}$
$\sigma_{(T_1-T_2)}$

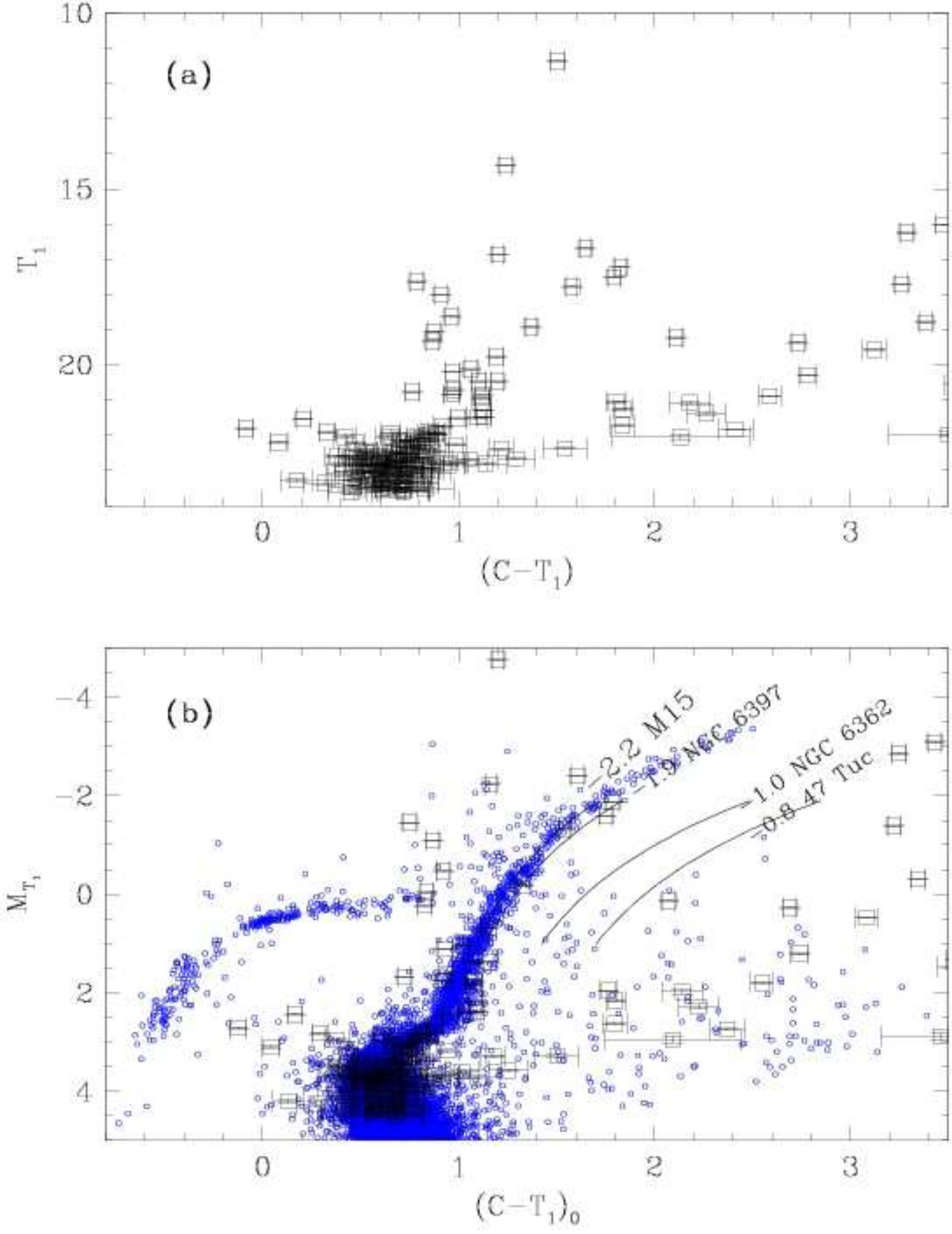
(a)
10
15
20
T_1
0
1
2
3
$(C-T_1)$
(b)
−4
−2
0
2
4
M_{T_1}
−2.2 M15
−1.9 NGC 6397
−1.0 NGC 6362
−0.8 47 Tuc
0
1
2
3
$(C-T_1)_0$

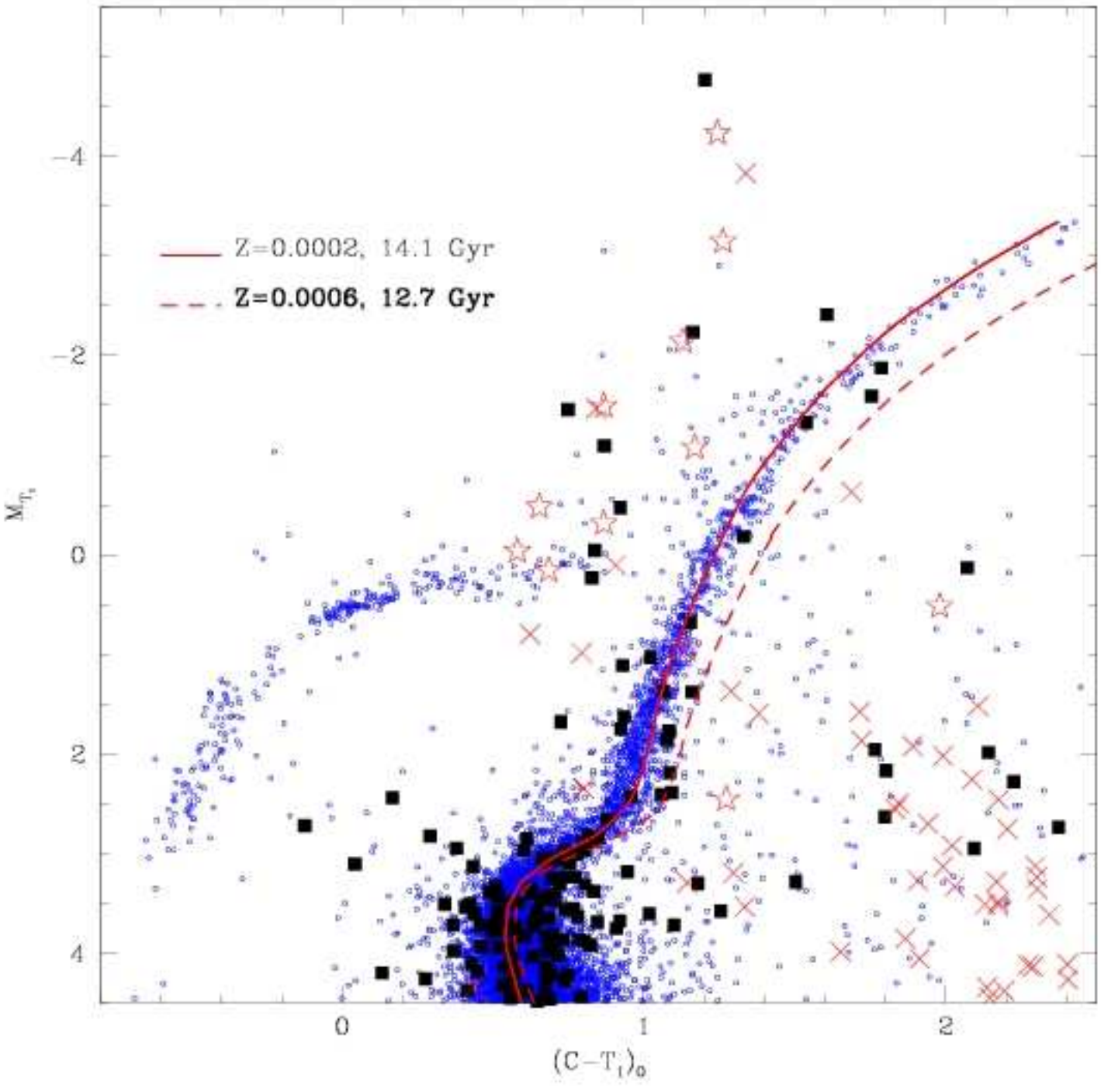
Z=0.0002, 14.1 Gyr
Z=0.0006, 12.7 Gyr
M_{T_1}
$(C-T_1)_0$
−4
−2
0
2
4
0
1
2

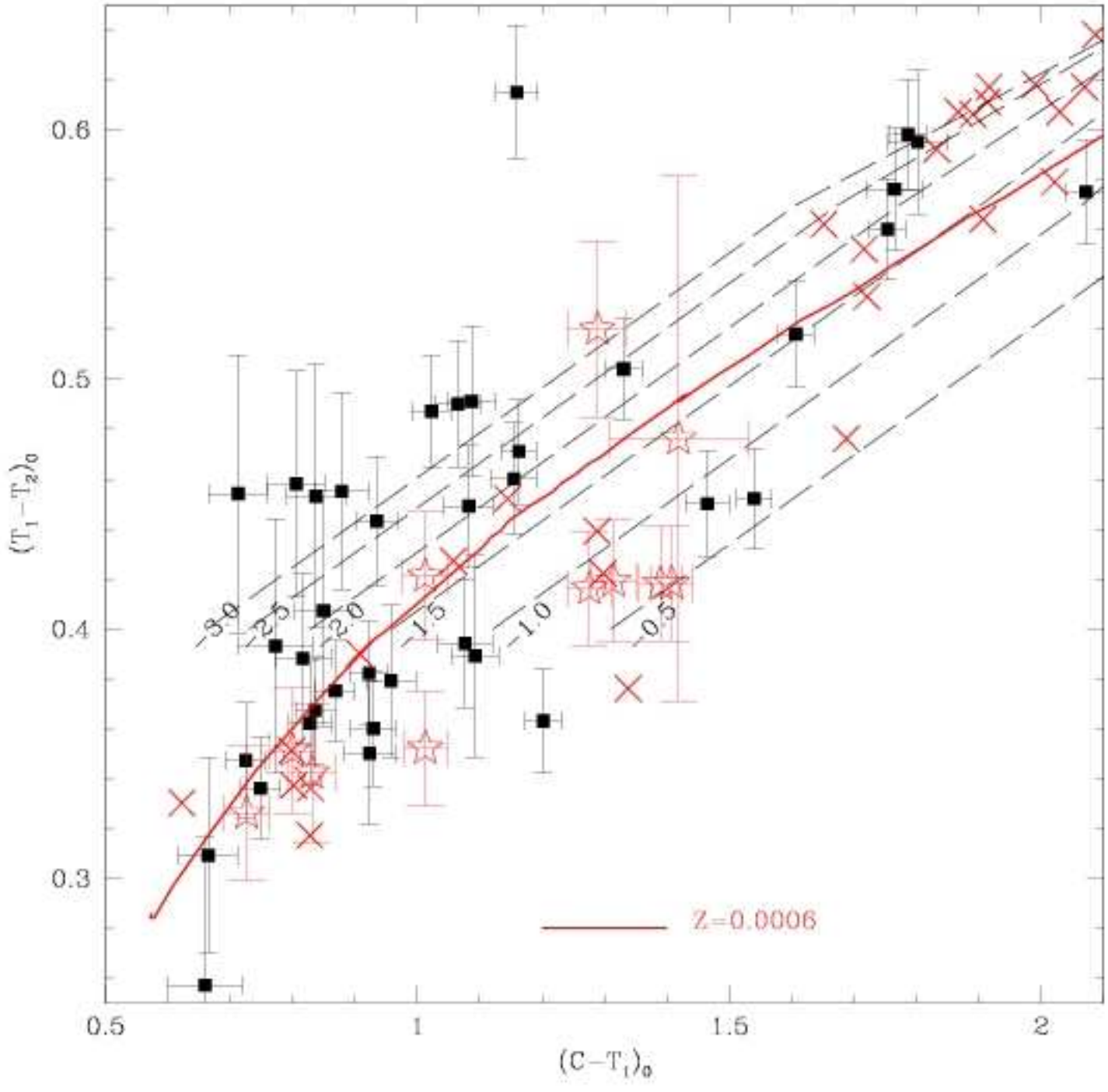
0.6
0.5
0.4
0.3
0.5
1
1.5
2
$(T_1-T_2)_0$
$(C-T_1)_0$
-3.0
-2.5
-2.0
-1.5
-1.0
-0.5
Z=0.0006

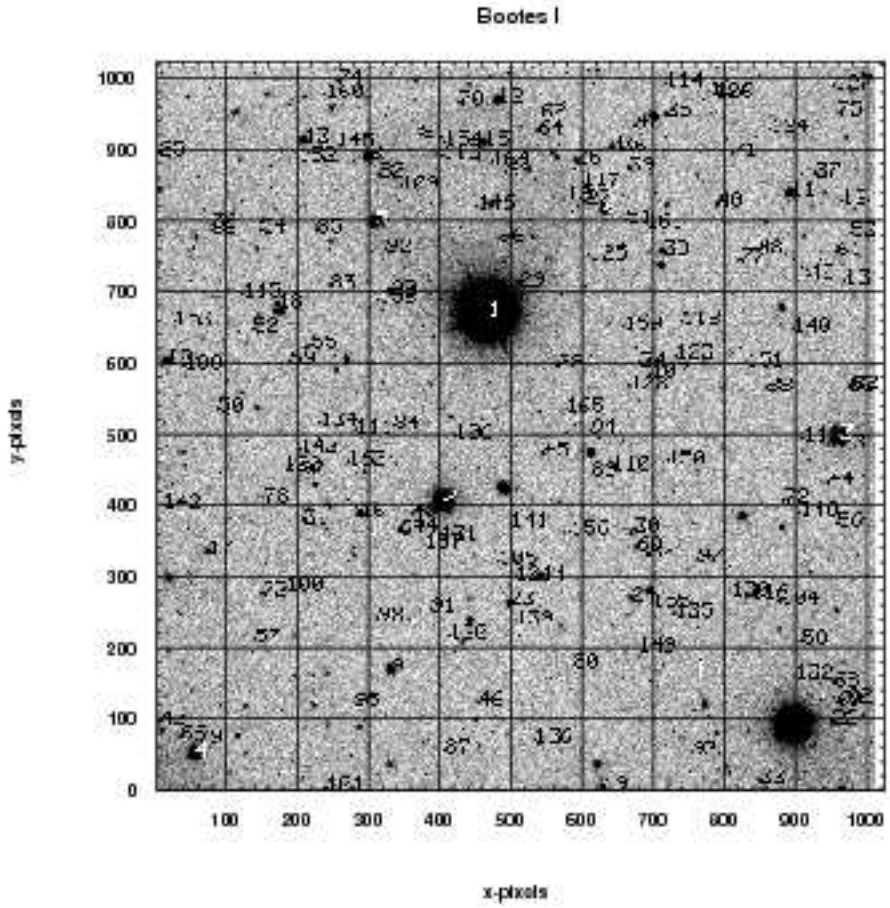
Bootes I
y-pixels
x-pixels
0
100
200
300
400
500
600
700
800
900
1000

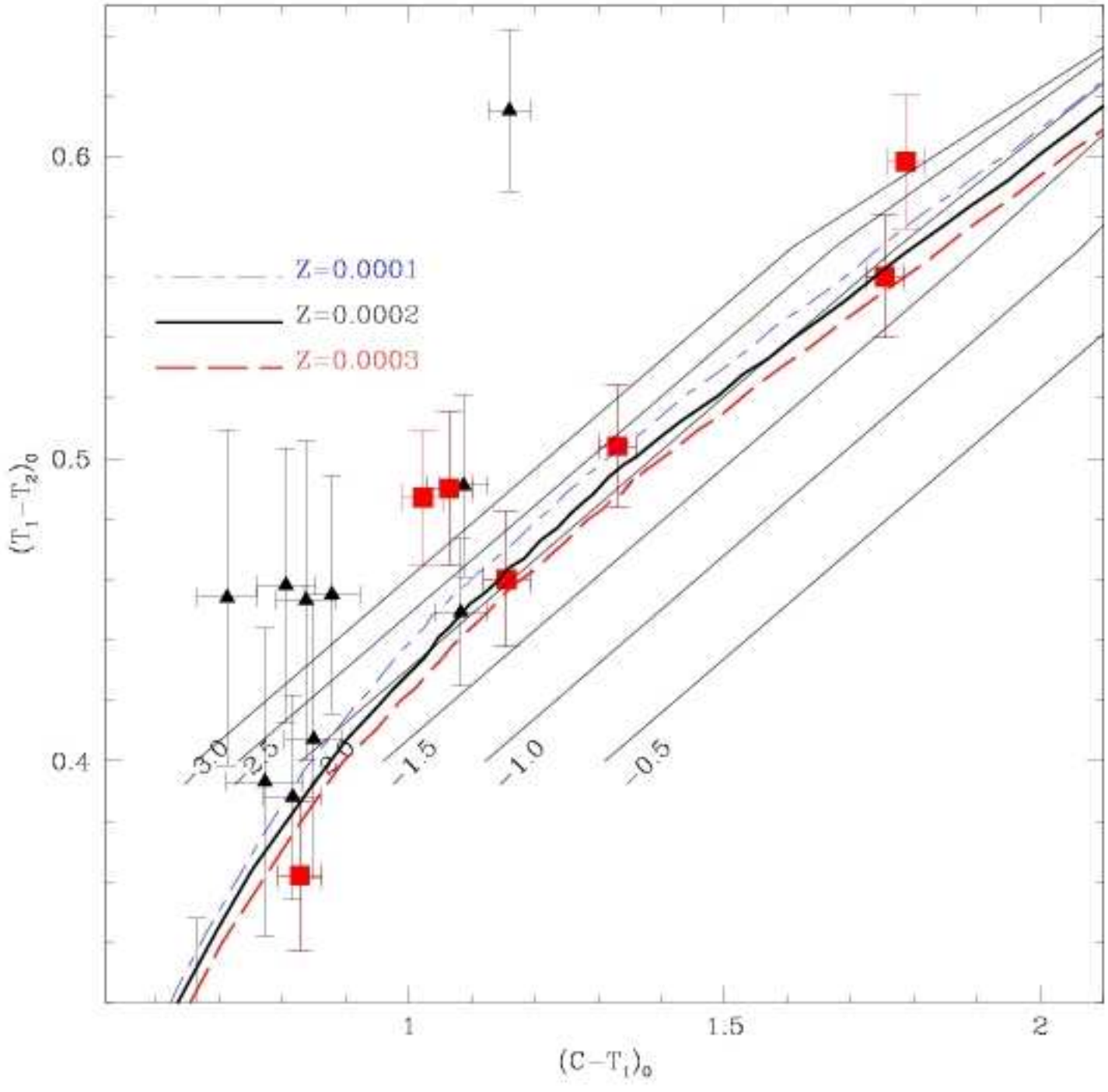
Z=0.0001
Z=0.0002
Z=0.0003
-3.0
-2.5
-2.0
-1.5
-1.0
-0.5
0.4
0.5
0.6
1
1.5
2
$(T_1-T_2)_0$
$(C-T_1)_0$

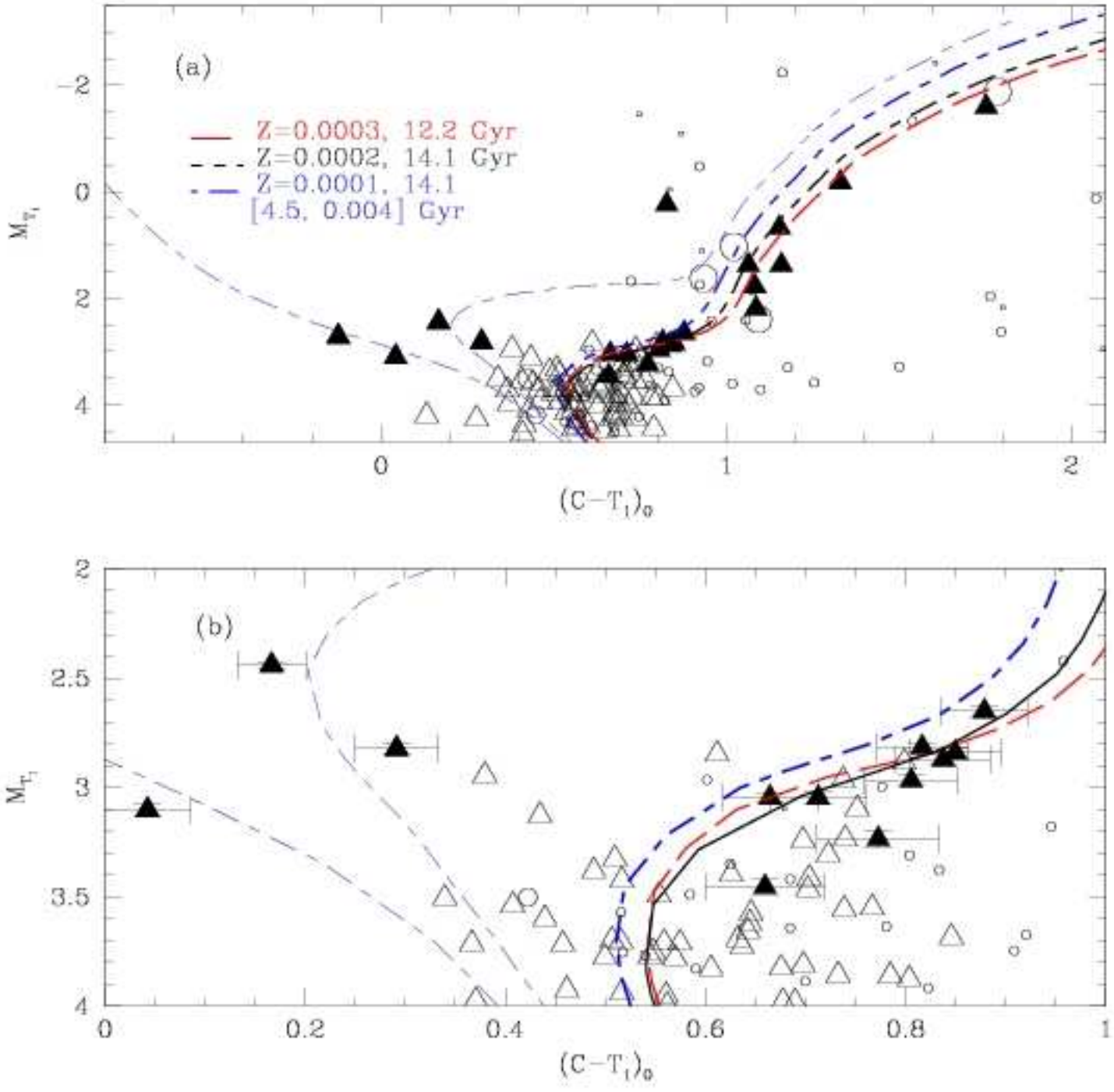
(a)
Z=0.0003, 12.2 Gyr
Z=0.0002, 14.1 Gyr
Z=0.0001, 14.1
[4.5, 0.004] Gyr
M_{T_1}
$(C-T_1)_0$
(b)
M_{T_1}
$(C-T_1)_0$